ORGANOMETALLICS

pubs.acs.org/Organometallics Article

Synthesis, Characterization, and Catalytic CO_2 Reduction Reactivity of Ruthenium CNC Pincer Complexes Containing Macrocyclic or Long Chain Wingtips

Weerachai Silprakob, Jannatul Ferdous, Sanjit Das, Jonah W. Jurss,* and Elizabeth T. Papish*

Cite This: *Organometallics* 2024, 43, 2077−2085 Read Online

ACCESS | Metrics & More | Article Recommendations | Supporting Information

ABSTRACT: Ruthenium CNC pincer complexes, comprised of *N*-heterocyclic carbenes (NHCs) and a pyridyl ring, are highly active catalysts for carbon dioxide reduction. We hypothesized that the addition of long chain aliphatic groups with an olefin terminus as wingtips on these CNC pincers could be used to form macrocyclic catalysts by ring closing metathesis (RCM). We have synthesized three new ruthenium pincer catalysts, $[(CNC)Ru(CH_3CN)_2Cl]OTf$, containing a long chain olefin wingtip (where the substituent *para* to N on the pyridine ring is H, Me, or OMe) and performed RCM on one compound with R = Me, followed by hydrogenation, to form a novel macrocyclic ruthenium catalyst. These four catalysts were tested for the photocatalytic reduction of carbon dioxide (CO_2) in the presence (sensitized) and absence (self-sensitized) of an external photosensitizer. With a photosensitizer, these catalysts produced mostly CO (775 to 1210 TON) with smaller amounts of H_2 also formed. The methyl substituted macrocyclic catalyst showed a TON of 1185 for CO over 72 h compared to a TON of 775 for CO for the analogous nonmacrocyclic catalyst. The remote substituents at the *para*-position of the central pyridine ring significantly influence catalyst activity with R = OMe > H ≈ Me.

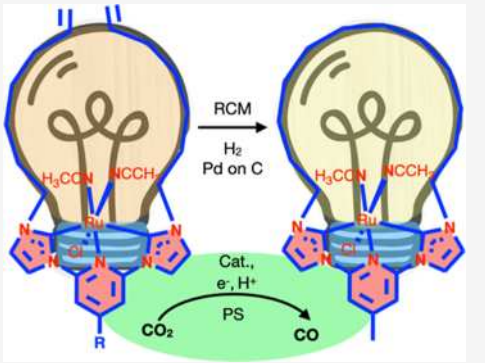

INTRODUCTION

The rising concentration of atmospheric carbon dioxide (CO_2) and its resultant global climate change have made the development of efficient and sustainable methods for CO_2 reduction an urgent priority.[1] One of the promising approaches for CO_2 reduction is the use of photocatalytic systems that can convert CO_2 to value-added chemicals using solar energy.[2−8] In our study, we directed our attention toward reducing carbon dioxide to carbon monoxide (CO) as a key objective, aimed at using CO and H_2 eventually in the Fischer−Tropsch process. This process is a well-established pathway for transforming CO into valuable liquid fuels with high energy density.[9] In this regard, homogeneous systems have been our focus due to ease of optimization and study to better understand the reaction mechanism.

Ruthenium-based catalysts offer a promising solution for CO_2 reduction due to their high activity, versatility, stability, and tunability.[10−12] Among different types of ruthenium catalysts, pincer ligand-based ruthenium catalysts (e.g., **7**, Figure 1)[11] have emerged as highly active and selective catalysts for various organic transformations[13] and have shown promising results in CO_2 reduction.[10−12,14−18] However, much remains to be learned about the factors that influence their catalytic performance and how they can be optimized for CO_2 reduction.[11,12,14−23] The *para*-substituent group on the pyridine ring (R in Figure 1) has proven to be one of the most important factors that can influence the performance of ruthenium pincer catalysts in the reduction of CO_2. The electronic character of the substituent group can significantly change the catalytic activity, selectivity, and stability of the catalyst.[11,12] For example, electron-donating R substituents, such as methyl or methoxy groups, can increase the electron density at the ruthenium center and enhance the catalytic activity of the catalyst toward CO_2 reduction. On the other hand, electron-withdrawing substituents such as chloro, trifluoromethyl, or nitro groups can decrease the electron density at the metal center,[24] but these substituents have rarely been used in the context of CO_2 reduction catalysis.[25]

Chaplin et al. reported on the reactivity of macrocyclic rhodium catalysts (Figure 1)[26,27] and explored the effect of ring size on stoichiometric alkyne coupling reactions.[28,29] The authors found that ring size has a significant impact on the reaction rate and regioselectivity due to ring strain and metal accessibility. Gladysz et al. have made significant contributions toward the synthesis and characterization of macrocyclic platinum, palladium, and rhodium complexes shaped like gyroscopes.[30−33] The rhodium complexes showed catalytic

Received: June 26, 2024
Revised: August 9, 2024
Accepted: August 20, 2024
Published: September 4, 2024

https://doi.org/10.1021/acs.organomet.4c00282
Organometallics 2024, 43, 2077−2085

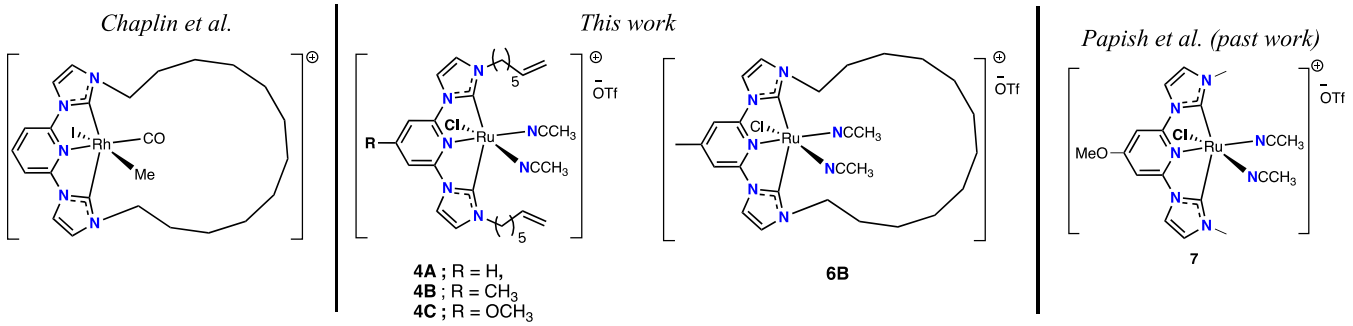

Figure 1. Past work by Chaplin et al. has used Rh and other metals in macrocyclic catalysts. In this work, we utilize Ru(II) as the metal center for both nonmacrocyclic and macrocyclic complexes.

Scheme 1. Synthetic Pathway to Formation of Macrocyclic Ru(II) Complexes[a]

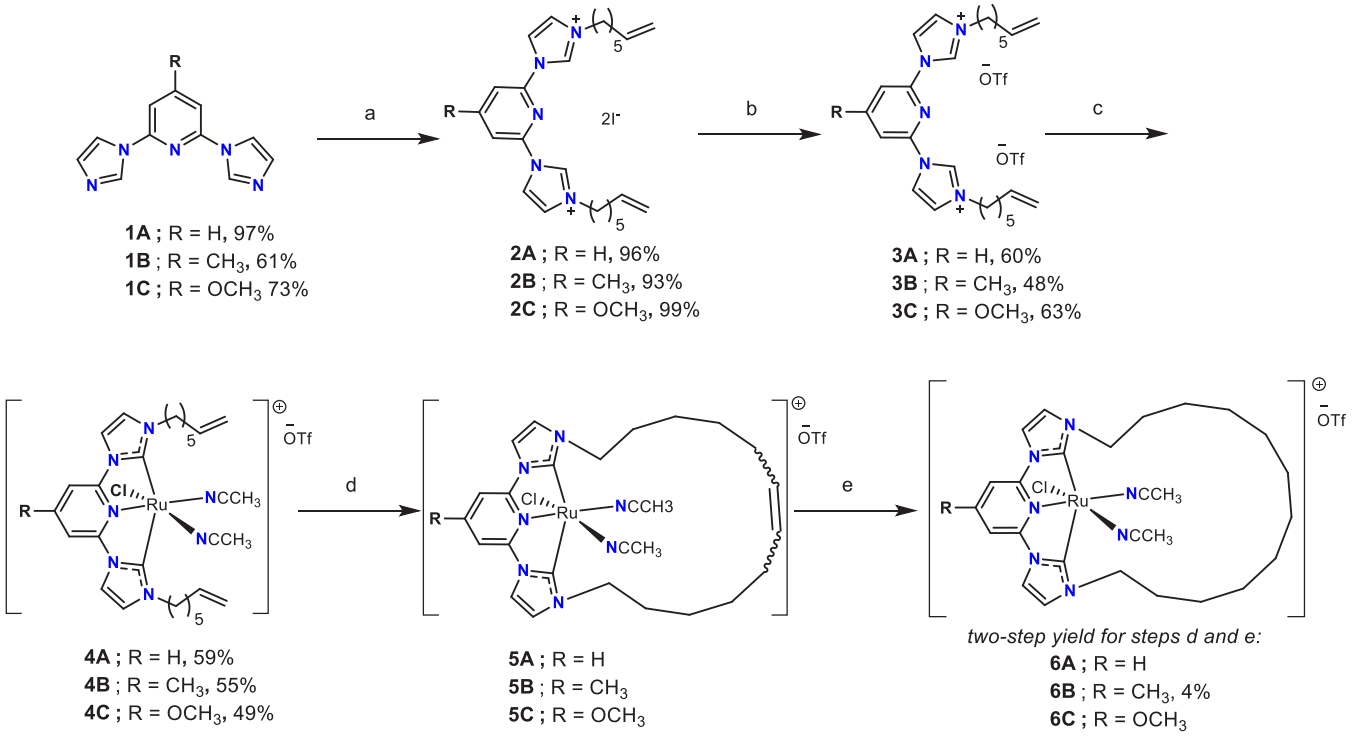

[a](a) 7-Iodo-1-heptene, DMF; (b) CF_3SO_3Ag, ethanol, 3 h; (c) $[Ru(\eta^6\text{-}p\text{-cymene})Cl_2]_2$, NEt_3, acetonitrile; (d) Grubbs first generation catalyst (benzylidene-bis(tricyclohexylphosphine)dichlororuthenium), CH_2Cl_2; (e) Pd/C, H_2, acetonitrile.

activity toward olefin hydroformylation.[30] Both the Chaplin and Gladysz groups have synthesized these macrocyclic ligands by the metal coordination reaction of ligands containing long aliphatic carbon chains with olefin end groups. The olefin end groups are then subjected to ring-closing metathesis and subsequent hydrogenation of the resulting double bond. We postulated that restricting the coordination sphere via the steric encumbrance provided by macrocyclic pincer ligands may serve to prevent decomposition reactions for Ru(II) CO_2 reduction catalysts. Thus, we have adapted these procedures to synthesize a macrocyclic version of our Ru(II) catalysts. Furthermore, the nonmacrocyclic precursors may also have enhanced catalytic activity due to the tendency of long chain aliphatic groups to aggregate in solution and potentially form catalytic micelles.[34]

In this manuscript, we report a new macrocyclic ruthenium catalyst $[(CNC)Ru(CH_3CN)_2Cl]OTf$ (**6B**) and three new ruthenium complexes with long chain olefin wingtips (**4A**-**4C**) for the photocatalytic reduction of CO_2 to CO (Figure 1). The CNC ligand is a tridentate pincer consisting of two imidazole-derived *N*-heterocyclic carbene (NHC) rings and a pyridyl ring, with R groups at the *para*-position (R = H, Me, and OMe). Due to synthetic difficulties in isolating **6A** and **6C**, we have chosen to focus this manuscript solely on catalysis with **4A**, **4B**, **4C**, and **6B**. Compound **7** (Figure 1) from our prior publication is also included in our discussion as a point of comparison for evaluating the role of the macrocyclic ring.[11]

RESULTS AND DISCUSSION

Synthesis. The present study outlines a synthetic procedure (Scheme 1) for producing the targeted macrocyclic Ru(II) product. The synthesis of the CNC pincer ligand precursors and the corresponding nonmacrocyclic ruthenium complexes have been previously reported and herein we use similar procedures.[12,14,15] Compounds **1A**-**1C** were alkylated via an S_N2 reaction with 7-iodoheptene (step a) to yield **2A**-**2C**

https://doi.org/10.1021/acs.organomet.4c00282
Organometallics 2024, 43, 2077−2085

which were subsequently treated with AgOTf (step b) to replace the iodide with a triflate counteranion to produce compounds **3A**-**3C** in moderate yields (48−63%, Scheme 1). Next, in step c, the CNC ligand precursor underwent deprotonation of the imidazolium ring by NEt_3 which led to formation of the NHC donors in the CNC pincer ligand which were metalated with $[Ru(\eta^6\text{-}p\text{-cymene})Cl_2]_2$.[11,12,14] This procedure generated the olefin containing ruthenium complexes **4A**-**4C** in 59, 55, and 49% yields, respectively. These products were characterized by ^{1}H NMR, ^{19}F NMR, and ultraviolet−visible (UV−vis) spectroscopies as well as by mass spectrometry (MS). The connectivity within **4C** was also confirmed by single crystal X-ray diffraction (SC-XRD) (Figure S38 in the Supporting Information). Disorder in the alkyl chains prevented modeling of all the carbon atoms at the end of the chain; therefore, this structure is of poor quality and would not be appropriate for analysis of bond lengths and angles. Ring-closing metathesis reactions were then performed (step d) on compounds **4A**-**4C** using the Grubbs first generation catalyst to yield **5A**-**5C**. Complexes **5A**-**5C** were not used directly for catalysis because a mixture of *cis* and *trans* isomers was present for each compound. In the final step, step e, complex **5B** underwent hydrogenation with H_2/Pd to yield the desired macrocyclic product **6B**, albeit with a low yield of 4% over two steps. However, the syntheses of analogous compounds **5A**, **5C**, **6A**, and **6C** were very low yielding and the isolation of these compounds proved challenging. Therefore, we have decided to focus solely on **6B** in this report.

UV−Visible Spectroscopy. The UV−visible absorption spectra of the long chain wingtip bearing (**4A**-**4C**) and macrocyclic (**6B**) Ru complexes show metal-to-ligand charge transfer (MLCT) bands from a Ru-based *d* orbital (HOMO) to the CNC π^* orbital (LUMO) centered on the pyridine ring, in analogy to previously published Ru complexes (Table 1 and Figure 2).[11,14] These MLCT bands were in the visible region (403−421 nm) and the UV region (351−359 nm) with all molar absorptivities (ε) around ∼5000 M^{-1} cm^{-1}. The visible absorption peaks are critical for light absorption during photocatalysis. We observe a blue shift in the MLCT bands in **4C** and **4B** relative to **4A** (e.g., 421, 414, and 403 nm for **4A**, **4B**, and **4C**, respectively) which is typical for the addition of an electron donor group (OMe or Me) which destabilizes the π^* based LUMO to a greater extent than the HOMO and thereby increases the energy of the transition.[11] The macrocyclic complex **6B** displays a similar UV−vis spectrum to its nonmacrocyclic analog **4B** with a slight blue-shift and a slight broadening of the peaks.

Table 1. UV−Vis Absorption Features for Each Complex (λ > 300 nm)

	λ (nm) (ε_{max} (M^{-1} cm^{-1}))	
complex	lower energy MLCT absorption band	higher energy MLCT absorption band
4A	421 (5(1) × 10^3)	356 (5(1) × 10^3)
4B	414 (5(1) × 10^3)	356 (5(1) × 10^3)
4C	403 (5(1) × 10^3)	359 (5(1) × 10^3)
6B	408 (4(1) × 10^3)	351 (4(1) × 10^3)

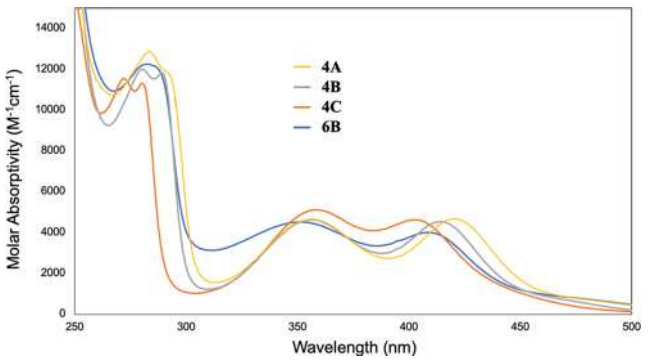

Figure 2. UV−vis absorption spectra for each Ru complex (0.02 mM) in acetonitrile.

Photocatalytic CO_2 Reduction. The Ru complexes were evaluated for their performance in the photochemical reduction of CO_2, both in the presence and absence of an external photosensitizer (PS). The strongly reducing PS, $Ir(ppy)_3$ (where ppy is 2-phenylpyridine), was applied as an external photosensitizer (−2.61 V vs $Fc^{+/0}$ in CH_3CN).[35] Photochemical experiments were performed with sacrificial electron donor 1,3-dimethyl-2-phenyl-2,3-dihydro-1*H*-benzimidazole (BIH), triethylamine (NEt_3) as a base to limit back electron transfer,[12] anhydrous acetonitrile (CH_3CN) as the solvent, and a light source (λ > 400 nm) adjusted to 1 Sun intensity. Control experiments were carried out to determine the necessity of each component in the photochemical system for CO_2 reduction (described below). Gas chromatography was used to quantify gaseous products such as carbon monoxide (CO), methane (CH_4), and hydrogen (H_2). We observed no formic acid by ^{1}H NMR, indicating that it is not a product in any of these reactions. The summary of photocatalysis with and without $Ir(ppy)_3$ PS is presented in Table 2.

Photocatalytic results are summarized and shown in Table 2 and Figure 3. At a concentration of 1 μM catalyst, in the presence of an external PS, the Ru complexes catalyze the reduction of CO_2 to primarily CO as the major product; one possible byproduct is CO_3^{2-} due to CO_2 disproportionation under anhydrous conditions.[10] Water is another likely

Table 2. Summary of Photocatalysis Results with and without an External PS[a,b]

catalyst	$Ir(ppy)_3$ PS (mM)	initial TOF (h^{-1})[c]	TON_{CO}	TON_{H_2}	TON_{CH_4}	CS (%)[d]
4C	0.1	101.7	1210	190	18	87
	0	5.3	19	38	23	53
6B	0.1	109.4	1185	267	18	82
	0	0.77	13	15	11	62
4A	0.1	95.6	827	448	9	65
	0	2.2	9	15	6	50
4B	0.1	163.1	775	306	0	72
	0	2.6	23	70	13	34
7	0.1[e]	174[e]	1006[e]	–[e]	–[e]	–[e]
	0[f]	0.5[f]	45[f]	–[f]	–[f]	–[f]

[a]The new complexes are arranged in order of decreasing TON of CO in the presence of $Ir(ppy)_3$. [b]Each catalyst was used in 1 μM concentration, unless otherwise noted. [c]Initial TOF (turnover frequency) was determined after 1 h irradiation. [d]Carbon Selective (CS) reduction percentage is calculated as [CS% = ((CO TON + CH_4 TON)/total product TON) × 100]. [e]Previously published. No formation of H_2, CH_4 or formate was observed.[11] [f]Previously published, catalyst concentration was 0.1 mM. No formation of H_2, CH_4 or formate was observed.[14]

https://doi.org/10.1021/acs.organomet.4c00282
Organometallics 2024, 43, 2077−2085

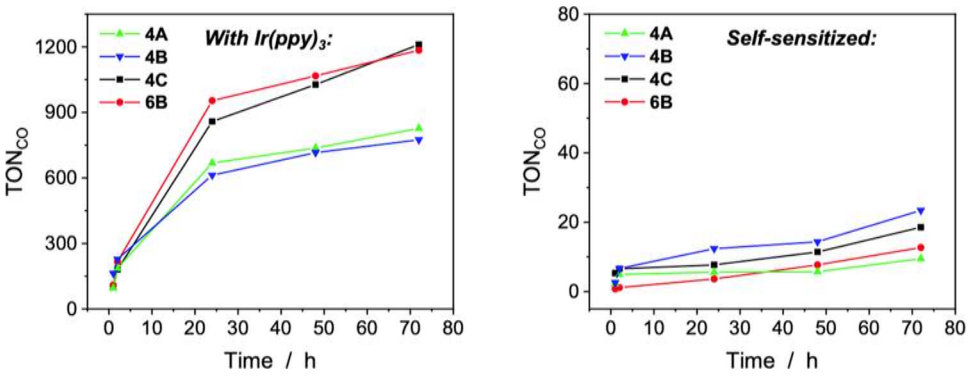

Figure 3. Photocatalytic CO production from CO_2 with 0.1 mM $Ir(ppy)_3$ PS (left) and under self-sensitized conditions (right) over 72 h period with catalysts **4A**, **4B**, **4C**, and **6B**. All experiments were performed in CH_3CN in the presence of 1 μM Ru catalyst, 11 mM BIH, and 5% (v/v) NEt_3 under a CO_2 atmosphere. All reported data points are the average of at least 2 experiments with ≤5% deviation from the average.

Table 3. Summary of Photocatalytic Control Experiments with Catalyst 4A[a]

entry	Cat **4A** (μM)	BIH (mM)	PS (mM)	NEt_3 (%)	atmosphere	TON_{CO}	TON_{H_2}	TON_{CH_4}
1	1	11	0.1	5	CO_2	827	448	9
2	0	11	0.1	5	CO_2	2	1	0
3	0	11	0.1	5	N_2	0	4	1
4	1	11	0.1	5	N_2	10	258	27
5	1	11	0.1	0	CO_2	137	19	9
6	1	0	0.1	5	CO_2	56	37	26
7	1	11	0	5	CO_2	9	15	5

[a]The irradiation time was held constant at 72 h. The activity under standard conditions is provided in Entry 1.

byproduct due to the acidity of BIH and NEt_3 after oxidation. H_2 is formed as a secondary product from proton reduction. CH_4 is also observed but it is not produced above the background TON value measured under N_2 (Table 3, entry 4). Interestingly, H_2 is the dominant product in the absence of an external photosensitizer (i.e., self-sensitized conditions).

Comparing **4A**, **4B**, and **4C**, catalyst **4C** with a methoxy substituent on the pyridine ring showed the best catalytic activity for CO_2 reduction, with turnover number (TON) for CO = 1210. Meanwhile, **4A** and **4B**, exhibited lower TON_{CO} values. The methoxy group in **4C** appears to enhance catalytic activity by electron donation via resonance and inductive effects.[36,37] The macrocyclic complex **6B** with a methyl substituent showed a TON_{CO} of 1185, surpassing the structurally related complex **4B**. Considering experimental error, **4C** and **6B** are comparable in activity with a PS present. This study demonstrates that electron-donating groups enhance the electron density at the metal center, promoting the activation of CO_2 and facilitating the formation of reactive intermediates during the reduction process.[19] Overall, the best catalysts herein (**4C** and **6B**) have similar TON_{CO} values to those previously reported for **7** with methyl wingtips (TON_{CO} = 1006, Figure 1 and Table 2).[11] The values for **7** may be within experimental error of those for **4C** and **6B**, since different lamps were used (both at 1 Sun intensity), which would seem to suggest that the significant synthetic efforts required to make **4C** and **6B** did not significantly enhance (or harm) the catalytic output of the Ru center. Thus, the long chain olefin wingtips and the macrocycle appear to be spectators in this reactivity. In terms of H_2 production (with PS present), the Ru complex **4A** exhibited the highest activity (TON_{H_2} = 448), followed by catalyst **4B**, and the lowest activity was observed for **6B** and **4C** (Table 2).

In self-sensitized photocatalysis, the complex functions as both the light absorber and the CO_2 reduction catalyst. Following excitation, the complex accepts an electron(s) from the sacrificial donor to undergo reduction and enter the catalytic cycle for CO_2 conversion.[12] Under these conditions, the studied Ru catalysts have relatively poor activity and lower selectivity for CO_2 reduction. Without an external PS, catalysts **4B** and **4C** (Me and OMe substituents, TON_{CO} = 23 and 19, respectively) had the highest activities and lower values are reported for the other catalysts. Prior work with **7** without an external PS is reported in Table 2, but we refrain from detailed analysis because there are significant differences in the conditions used ([**7**] = 0.1 mM vs 1 μM for the other catalysts).[14] For H_2 production, catalyst **4B** showed significant proton reduction activity, yielding a TON_{H_2} of 70.

A Hg drop homogeneity study of the most active catalyst, **4C**, was conducted by adding mercury to the reaction mixture 4 h after the reaction was initiated. Nearly identical photocatalytic activity was observed with or without the addition of mercury in the reaction mixture (Figure S39 in the Supporting Information) suggesting that the photocatalytic activity is due to a homogeneous molecular catalyst.[38] Results of the homogeneity experiment are presented in Table S1 in the Supporting Information.

The initial rate of catalysis (TOF) was also determined for each catalyst after 1 h irradiation, and they decrease in the order: **4B** (163.1 h^{-1}) > **6B** ≃ **4C** > **4A** (Table 2, with PS). It is worth noting that catalyst **4B**, which has the highest initial TOF, has the lowest TON_{CO} value of 775; its lower stability may be a consequence of its higher reactivity. Under self-sensitized photocatalytic conditions, much lower initial TOFs were observed (as high as 5.3 h^{-1} for **4C**). Importantly, there is no observable induction period for any of the complexes as

https://doi.org/10.1021/acs.organomet.4c00282
Organometallics 2024, 43, 2077−2085

catalysis begins immediately upon irradiation, which is further evidence of the molecular nature of these catalysts.

To assess the impact of each component in the photochemical system on catalysis, control experiments were conducted using complex **4A**. The results of these experiments are summarized in Table 3 where Entry 1 uses standard conditions, and each subsequent entry has had one component removed. In the absence of the ruthenium catalyst (Entries 2 and 3), under CO_2 or N_2 atmosphere, very little product is formed, clearly indicating that the catalyst is necessary. Similarly, the removal of any essential component (CO_2, NEt_3, BIH, or PS in entries 4−7) greatly decreases CO production. BIH is a potent sacrificial electron donor due to its relatively high oxidation potential.[39] NEt_3 can also serve as a sacrificial electron donor and as a proton source following oxidation, but it is less potent than BIH and its primary role is to function as a base to deprotonate $BIH^{\bullet+}$ to limit back electron transfer from the reduced PS.[12,39]

CONCLUSIONS

This study reports the synthesis and characterization of a series of ruthenium pincer complexes with long chain olefin wingtips and one macrocyclic ruthenium pincer complex. These four complexes were evaluated in the photocatalytic reduction of CO_2 to CO with and without a photosensitizer, $Ir(ppy)_3$. Overall, the Ru complexes were more efficient in the presence of a photosensitizer, and they produced mostly CO with small amounts of H_2. The long chain wingtip complexes showed activity that decreased in the order **4C** (TON_{CO} = 1210) > **4A** ≈ **4B** which shows that an electron donor group enhances catalytic activity in agreement with our past studies.[11,12,15] Comparing **4B** and **6B**, we observe that forming a macrocyclic ring reduces the initial TOF but improves the catalyst longevity leading to a higher TON for CO formation. Overall, these catalysts have similar TON values to previously reported analogs with methyl wingtips (TON = 1006 for **7**, Figure 1).[11] The mechanism of CO_2 reduction with Ru complexes similar to **7** have been studied by experimental and computational methods, and it appears that reduction of a $[(CNC)(bpy)Ru\text{-}CO_2]^+$ complex and subsequent C−O bond cleavage is turnover limiting.[40] These steps may be somewhat insensitive to the nature of the aliphatic wingtips groups. Thus, the synthesis of **4A**-**4C** and **6B** adds several synthetic steps with relatively minor improvements in TON values. Macrocyclic catalysts may prove to be more beneficial with other metals (e.g., first-row transition metals) that are more vulnerable to decomposition reactions, but with Ru there is only a modest benefit.

EXPERIMENTAL SECTION

General Considerations. Unless otherwise stated, reactions are prepared and performed under an inert atmosphere (N_2) using glovebox or Schlenk line techniques in oven-dried glassware. Workup and purifications are done open to the air.

Solvents and Reagents. Dry solvents (commercial or dried on a glass contour solvent purification system built by Pure Process Technology, LLC) are used for reactions unless described otherwise. Reagent-grade solvents are used for workup and purification. All the reagents are used as received from the commercial supplier without further purification. 2,6-difluoro-4-methoxypyridine is prepared as described in the literature.[41]

Instruments and Services. NMR spectra are recorded in a Bruker AVANCE 360 (360 MHz, ^1H frequency) or AVANCE 500 (500 MHz, ^1H frequency) NMR spectrometer. Fourier-transform infrared (FT-IR) spectra are recorded in a Bruker α ATRIR spectrophotometer. Mass spectra are obtained in a Waters AutoSpec-Ultima NT mass spectrometer or Waters Xero G2-XS QTOF. Electrochemical analysis was conducted with a CH Instruments potentiostat (CHI-600E). UV−visible spectra were recorded with an Ocean Optics FLAME-CHEM-UV−vis instrument and a cuvette with a 1 cm path length in the ambient atmosphere.

NMR Chemical Shift Reference. ^1H and $\{^1H\}^{13}C$ chemical shifts are assigned concerning the residual peaks from deuterated NMR solvents.[42] No reference is used for ^{19}F chemical shifts; only the number of peaks was checked.

SC-XRD Structure Determination. A crystal structure is included in the Supporting Information for connectivity only; the structure was not of sufficient quality to determine bond lengths and angles accurately. The long alkyl groups (wingtip) were not fully modeled to their full chain due to disorder. CCDC Deposition Number 2367435 contains the supporting crystallographic data for this paper. These data are provided free of charge by the joint Cambridge Crystallographic Data Centre and Fachinformationszentrum Karlsruhe Access Structures service www.ccdc.cam.ac.uk/structures.

Crystallographic data were collected from samples mounted on a MITIGEN holder in a XtaLAB Synergy R. DW system, HyPix diffractometer. During data collection, the crystals were kept at a steady T = 100.00(10) K. The structure was solved with the ShelXT solution program[43] using dual methods and by using Olex2 as the graphical interface.[44] The models were refined with ShelXL 2018/3[45] using full matrix least-squares minimization on F^2.

Synthesis and Characterization. *Synthesis of 7-Iodo-1-heptene.* An oven-dried Schlenk flask was loaded with NaI (5.90 g, 39.4 mmol, 2.0 equiv) and a stir-bar and sealed with a rubber septum; the flask was connected to a Schlenk line under N_2. The flask was evacuated and filled back with N_2, and this procedure was repeated three times. Dry acetone (30 mL) was transferred to the flask using a syringe through the septum. The reaction mixture was stirred to dissolve NaI, and as it dissolved, 7-bromo-1-heptene (3.49 g, 19.7 mmol, 1.0 equiv) was added to the flask using a syringe through the septum. Then the reaction mixture was stirred at 50 °C for 24 h. After cooling to room temperature, the reaction mixture was filtered through a Celite plug, the filtrate was evaporated to dryness, and the residue was dissolved in diethyl ether (50 mL) and washed with water. The water layer was extracted with diethyl ether (2 × 50 mL), the combined ether part was washed with brine, dried with Na_2SO_4, filtered, and the filtrate was evaporated to give the product, 7-iodo-1-heptene (4.25 g, 18.9 mmol, 96%) as a colorless oil. ^1H NMR ($CDCl_3$, 360 MHz): δ 5.86−5.75 (m, 1H); 5.04−4.94 (m, 2H); 3.19 (t, 2H, J_{H-H} = 7.2 Hz); 2.09−2.04 (m, 2H); 1.86−1.80 (m, 2H); 1.44−1.39 (m, 4H).

Synthesis of 1A. A Schlenk flask was loaded with 2,6-difluoropyridine (1.268 g, 11.02 mmol, 1.0 equiv), 1*H*-imidazole (1.876 g, 27.55 mmol, 2.5 equiv), K_2CO_3 (6.10 g, 44.07 mmol, 4.0 equiv) and a stir-bar. The flask was filled with DMF (20 mL) from the solvent purification system (SPS). Then, the flask was connected to a Schlenk line under N_2 and sealed with a rubber septum. The reaction mixture was stirred while heating at 80 °C for 16 h. After cooling to room temperature, the reaction mixture was filtered through a Celite plug with ethyl acetate. The filtrate was concentrated to get the crude product and purified by column chromatography using 0−8% methanol in dichloromethane as eluent to obtain the product (**1A**) as a white solid (2.269 g, 10.74 mmol, 97%). ^1H NMR ($CDCl_3$, 360 MHz): δ 8.38 (s, 2H); 7.97 (t, 1H, J = 7.2 Hz); 7.67 (s, 2H); 7.29 (d, 2H, J = 7.2 Hz); 7.24 (s, 2H).

Synthesis of 2A. An oven-dried round-bottom flask was loaded with 2,6-di(1*H*-imidazol-1-yl)-pyridine (0.30 g, 1.42 mmol, 1.0 equiv), 7-iodo-1-heptene (**1**) (1.59 g, 7.10 mmol, 5.0 equiv), DMF (30 mL) and a stir-bar. The flask was sealed with a rubber septum, and the reaction mixture was stirred at 70 °C for 24 h in an N_2 environment. After cooling to room temperature, the reaction mixture was evaporated to dryness. The residue was triturated with dichloromethane (2 mL) and diethyl ether (30 mL) to get a

https://doi.org/10.1021/acs.organomet.4c00282
Organometallics 2024, 43, 2077−2085

yellowish-orange wax-like solid, and the solvent was decanted. The solid was washed with diethyl ether (2 × 30 mL) to obtain the desired product (**2A**) (0.90 g, 1.36 mmol, 96%). ^{1}H NMR ($CDCl_3$, 360 MHz): δ 11.25 (s, 2H); 8.83 (s, 2H); 8.49 (s, 3H); 7.75 (s, 2H); 5.80−5.69 (m, 2H); 4.99−4.89 (m, 4H); 4.61 (t, 4H, J_{H-H} = 7.2 Hz); 2.05 (m, 8H); 1.46 (m, 8H).

Synthesis of ***3A***. Compound **2A** (0.573 g, 0.95 mmol, 1.0 equiv) was dissolved in ethanol (15 mL) in an oven-dried round-bottom flask. To this solution was added a solution of CF_3SO_3Ag (0.488 g,1.90 mmol, 2.0 equiv) in ethanol (5 mL), and the resulting mixture was stirred at room temperature in an N_2 environment for 3 h. Then the reaction mixture was filtered through a Celite plug; the filtrate was evaporated to dryness. The residue was triturated with acetonitrile (1 mL) and diethyl ether (20 mL) to get a yellowish-orange wax-like solid. The solid was further washed with diethyl ether (20 mL) to obtain the desired product (**3A**) (0.367 g, 0.57 mmol, 60%). ^{1}H NMR ($CDCl_3$, 360 MHz): δ 11.25 (s, 2H); 8.83 (s, 2H); 8.49 (s, 3H); 7.75 (s, 2H); 5.80−5.69 (m, 2H); 4.99−4.89 (m, 4H); 4.61 (t, 4H, J_{H-H} = 7.2 Hz); 2.05 (m, 8H); 1.46 (m, 8H).

Synthesis of ***4A***. Inside the glovebox, an oven-dried Schlenk flask was loaded with $[Ru(p\text{-Cym})Cl_2]_2$ (0.183 g, 0.30 mmol, 1.0 equiv), 1,1′-(pyridine-2,6-diyl)bis(3-(hept-6-en-1-yl)-1*H*-imidazol-3-ium)-ditriflate (0.400 g, 0.569 mmol, 1.9 equiv), acetonitrile (50 mL) and a stir-bar, the flask was sealed with a rubber septum, taken out of the box and connected to a Schlenk line under N_2. Triethylamine (0.209 mL, 1.50 mmol, 5.0 equiv) was added to the flask using a syringe through the septum. Then the reaction mixture was stirred at 60 °C for 24 h. After cooling to room temperature, the reaction mixture was concentrated to get the crude product as a brownish-yellow solid. The crude product was subjected to column chromatography on silica gel using 0−10% methanol in dichloromethane to get a yellow solid. The solid was triturated three times with a solvent mixture of dichloromethane (1 mL) and diethyl ether (5 mL), the supernatant solution was decanted, and the solid was further washed with diethyl ether (10 mL) to obtain the yellow solid product (**4A**) (0.257 g, 0.333 mmol, 59%). The data supports the presence of triflate as the counteranion based upon ^{19}F NMR and MS in anion mode, but we cannot rigorously rule out the presence of some adventitious chloride anion which would reduce the molecular weight and alter the catalysis TON values slightly. ^{1}H NMR ($CDCl_3$, 360 MHz, ppm): δ 7.77−7.75 (m, 3H); 7.34 (d, 2H, J_{HH} = 10.8 Hz); 7.18 (d, 2H, J_{HH} = 3.6 Hz); 5.83−5.76 (m, 2H); 5.04−4.94 (m, 4H); 4.58−4.41 (m, 4H); 2.66 (s, 3H); 2.07−2.01 (m, merged peaks, 11H); 1.50−1.49 (m, 8H). ^{19}F NMR ($CDCl_3$, 339 MHz, ppm): δ −78.16. HRMS (ESI, positive) calcd for $RuC_{29}H_{39}N_7OCl$ $[M - (CF_3SO_3)^-]^+$: 622.2003 and found 622.2017. UV−vis: λ_{max} = 358 nm, 418 nm. FTIR (ATR, cm^{-1}): 3079, 2928, 2857, 2273 (CN of nitrile), 1639 (C═C or C═N).

Synthesis of ***1B***. A Schlenk flask was loaded with 2,6-dichloro-4-methylpyridine (3.00 g, 18.52 mmol, 1.0 equiv), 1*H*-imidazole (2.774 g, 40.74 mmol, 2.2 equiv), K_2CO_3 (10.24 g, 78.08 mmol, 4.0 equiv) and a stir-bar. The flask was filled with DMF (60 mL) from the SPS. Then, the flask was connected to a Schlenk line under N_2 and sealed with a rubber septum. The reaction mixture was stirred while heating at 100 °C for 48 h. After cooling to room temperature, the reaction mixture was filtered through Celite plug with ethyl acetate. Filtrate was concentrated to get the crude product and purified by column chromatography using 0−10% methanol in dichloromethane as eluent to obtain the product (**1B**) as a white solid (2.56 g, 11.36 mmol, 61%). ^{1}H NMR ($CDCl_3$, 360 MHz): δ 8.36 (s, 2H); 7.66 (s, 2H,); 7.23 (s, 2H); 7.11 (d, 2H); 2.54 (s, 3H).

Synthesis of ***2B***. An oven-dried round-bottom flask was loaded with 2,6-di(1*H*-imidazol-1-yl)-4-methylpyridine (0.60 g, 2.66 mmol, 1.0 equiv), 7-iodo-1-heptene (**1**) (2.61 g, 13.32 mmol, 5.0 equiv), DMF (30 mL) and a stir-bar. The flask was sealed with a rubber septum, and the reaction mixture was stirred at 70 °C for 24 h in an N_2 environment. After cooling to room temperature, the reaction mixture was evaporated to dryness. The residue was triturated with dichloromethane (2 mL) and diethyl ether (30 mL) to get a yellowish-orange wax-like solid, and the solvent was decanted. The solid was washed with diethyl ether (2 × 30 mL) to obtain the desired product (**2B**) (1.66 g, 2.64 mmol, 93%). ^{1}H NMR ($CDCl_3$, 360 MHz): δ 11.47 (s, 2H); 8.86 (s, 2H); 8.42 (s, 2H); 7.59 (s, 2H); 5.81−5.73 (m, 2H); 5.01−4.93 (m, 4H); 4.64−4.61 (m, 4H,); 2.74 (s, 3H); 2.08−2.06 (m, 8H); 1.49−1.45 (m, 8H).

Synthesis of ***3B***. Compound **2B** (0.47 g, 0.764 mmol, 1.0 equiv) was dissolved in ethanol (30 mL) in an oven-dried round-bottom flask. To this solution was added a solution of CF_3SO_3Ag (0.39 g, 1.53 mmol, 2.0 equiv) in ethanol (30 mL), and the resulting mixture was stirred at room temperature in an N_2 environment for 3 h. Then the reaction mixture was filtered through a Celite plug; the filtrate was evaporated to dryness. The residue was triturated with acetonitrile (1 mL) and diethyl ether (20 mL) to get a yellowish-orange wax-like solid. The solid was further washed with diethyl ether (20 mL) to obtain the desired product (**3B**) (0.28 g, 0.39 mmol, 48%). ^{1}H NMR ($CDCl_3$, 360 MHz): δ 10.34 (s, 2H); 8.53 (s, 2H); 7.97 (s, 2H); 7.52 (s, 2H); 5.81−5.70 (m, 2H); 5.00−4.92 (m, 4H); 4.42 (t, 4H, J_{H-H} = 7.2 Hz); 2.60 (s, 3H); 2.07−1.89 (m, 8H); 1.49−1.35 (m, 8H). ^{19}F NMR ($CDCl_3$, 339 MHz): δ −78.48.

Synthesis of ***4B***. Inside the glovebox, an oven-dried Schlenk flask was loaded with $[Ru(p\text{-Cym})Cl_2]_2$ (0.126 g, 0.20 mmol, 1.0 equiv), 1,1′-(4-methylpyridine-2,6-diyl)bis(3-(hept-6-en-1-yl)-1*H*-imidazol-3-ium)ditriflate (0.280 g, 0.39 mmol, 1.9 equiv), acetonitrile (50 mL) and a stir-bar, the flask was sealed with a rubber septum, taken out of the box and connected to a Schlenk line under N_2. Triethylamine (0.140 mL, 1.00 mmol, 5.0 equiv) was added to the flask using a syringe through the septum. Then the reaction mixture was stirred at 60 °C for 24 h. After cooling to room temperature, the reaction mixture was concentrated to get the crude product a brownish-yellow solid. The crude product was subjected to column chromatography on silica gel using 0−10% methanol in dichloromethane to get a yellow solid. The solid was triturated three times with a solvent mixture of dichloromethane (1 mL) and diethyl ether (5 mL), the supernatant solution was decanted, and the solid was further washed with diethyl ether (10 mL) to obtain the yellow solid product (**4B**) (0.167 g, 0.212 mmol, 55%). The data supports the presence of triflate as the counteranion based upon ^{19}F NMR and MS in anion mode, but we cannot rigorously rule out the presence of some adventitious chloride anion which would reduce the molecular weight and alter the catalysis TON values slightly. ^{1}H NMR ($CDCl_3$, 360 MHz, ppm): δ 7.73 (d, 2H, J_{HH} = 1.8 Hz); 7.20 (s, 2H,); 7.16 (d, 2H, J_{HH} = 2.1 Hz); 5.83−5.76 (m, 2H); 5.03−4.94 (m, 4H); 4.54−4.40 (m, 4H); 2.64 (merged peaks, 6H); 2.09−2.06 (m, 11H); 1.49−1.47 (m, 8H). ^{19}F NMR ($CDCl_3$, 339 MHz, ppm): δ − 78.18. HRMS (ESI, positive) calcd for $RuC_{30}H_{41}N_7OCl$ $[M - (CF_3SO_3)^-]^+$: 626.1953 and found 626.1946. UV−vis: λ_{max} = 357 nm, 412 nm. FTIR (ATR, cm^{-1}): 3089, 2927, 2857, 2267 (CN of nitrile), 1628 (C═C or C═N).

Synthesis of ***5B***. This synthesis was carried out in a similar fashion to a literature procedure.[26] Inside the glovebox, an oven-dried Schlenk flask was loaded with **4B** (0.100 g, 0.127 mmol, 1.0 equiv), Grubbs first generation catalyst (benzylidene-bis(tricyclohexylphosphine)-dichlororuthenium) (0.011 g, 0.013 mmol, 0.1 equiv), dichloromethane (70 mL), and a stir-bar, the flask was sealed with a rubber septum, taken out of the box and connected to a Schlenk line under N_2. The reaction mixture was stirred at room temperature for 3 days. The reaction mixture was concentrated to get the crude product as a brownish-yellow solid. The crude product was subjected to column chromatography on silica gel using 7:2:1 dichloromethane: acetonitrile: methanol to get a mixture of **5B** (15 mg, 0.020 mmol, 16%), no further purification.

Synthesis of ***6B***. This synthesis was carried out in a similar fashion to a literature procedure.[26] An oven-dried Schlenk flask was loaded with **5B** (0.015 g, 0.020 mmol, 1.0 equiv), Pd/C (0.001 g, 0.002 mmol, 0.1 equiv), 10 mL of acetonitrile, a stir-bar, and sealed with a rubber septum, the flask was connected to a Schlenk line under vacuum. The flask was filled with H_2 gas and was stirred at room temperature for 3 days. The reaction mixture was filtered through a Celite plug; the filtrate was evaporated to dryness to give the crude product. HPLC purified the crude product to obtain **6B** (4 mg, 0.005 mmol, 25%) as a yellow solid. The data supports the presence of triflate as the counteranion based upon ^{19}F NMR and MS in anion

https://doi.org/10.1021/acs.organomet.4c00282
Organometallics 2024, 43, 2077−2085

mode, but we cannot rigorously rule out the presence of some adventitious chloride anion which would reduce the molecular weight and alter the catalysis TON values slightly. ^{1}H NMR ($CDCl_3$, 360 MHz, ppm): δ 7.87 (d, 2H, J_{HH} = 1.8 Hz); 7.39 (s, 2H,); 7.33 (d, 2H, J_{HH} = 2.1 Hz); 4.66−4.60 (m, 2H); 4.23−4.17 (m, 2H); 2.60 (s, 3H); 2.59 (s, 3H); 2.13 (merged peak, 3H). ^{19}F NMR ($CDCl_3$, 339 MHz, ppm): δ − 79.33. HRMS (ESI, positive) calcd for $RuC_{28}H_{39}N_7Cl$ [M − $(CF_3SO_3)^-$]$^+$: 610.2003 and found 610.2020. UV−vis: λ_{max} = 357 nm, 412 nm. FTIR (ATR, cm^{-1}): 3114, 2920, 2851, 2267 (CN of nitrile), 1629 (C═C or C═N).

Synthesis of ***1C***. A Schlenk flask was loaded with 2,6-difluoro-4-methoxypyridine (2.36 g, 16.3 mmol, 1.0 equiv), 1*H*-imidazole (2.26 g, 33.3 mmol, 2.05 equiv), NaH (0.798 g, 33.3 mmol, 2.05 equiv) and a stir-bar. The flask was filled with DMF (125 mL) from the SPS. Then, the flask was connected to a Schlenk line under N_2 and sealed with a rubber septum. The reaction mixture was stirred while heating at 70 °C for 16 h. After cooling to room temperature, the reaction mixture was filtered through a Celite plug, followed by solvent removal by rotary evaporation to give the yellow solid as a crude product. The solid was purified by crystallization in 40 mL of EtOH, resulting in a white solid. The white solid was collected by filtration and washed with minimal cold EtOH followed by diethyl ether to obtain the product ($\mathbf{1}_C$) as a white solid (2.90 g, 11.9 mmol, 73%). ^{1}H NMR (DMSO, 360 MHz): δ 8.73 (s, 2H); 8.12 (s, 2H); 77.34 (s, 2H); 7.12 (s, 2H); 3.99 (s, 3H).

Synthesis of ***2C***. An oven-dried round-bottom flask was loaded with 2,6-di(1*H*-imidazol-1-yl)-4-methoxypyridine (1.00 g, 4.14 mmol, 1.0 equiv), 7-iodo-1-heptene (**1**) (4.64 g, 20.7 mmol, 5.0 equiv), DMF (50 mL) and a stir-bar. The flask was sealed with a rubber septum, and the reaction mixture was stirred at 70 °C for 24 h in an N_2 environment. After cooling to room temperature, the reaction mixture was evaporated to dryness. The residue was triturated with dichloromethane (2 mL) and diethyl ether (30 mL) to get a yellowish-orange wax-like solid, and the solvent was decanted. The solid was washed with diethyl ether (2 × 30 mL) to obtain the desired product (**2C**) (2.69 g, 3.90 mmol, 99%). ^{1}H NMR ($CDCl_3$, 360 MHz): δ 11.45 (s, 2H); 8.98 (s, 2H); 7.84 (s, 2H); 7.63 (s, 2H); 5.81−5.70 (m, 2H); 5.01−4.91 (m, 4H); 4.63 (t, 4H, J_{H-H} = 7.2 Hz); 4.29 (s, 3H); 2.05 (m, 8H); 1.45 (m, 8H).

Synthesis of ***3C***. Compound **2C** (1.47 g, 2.14 mmol, 1.0 equiv) was dissolved in ethanol (40 mL) in an oven-dried round-bottom flask. To this solution was added a solution of CF_3SO_3Ag (1.10 g, 4.28 mmol, 2.0 equiv) in ethanol (20 mL) and the resulting mixture was stirred at room temperature in an N_2 environment for 3 h. Then the reaction mixture was filtered through a Celite plug, the filtrate was evaporated to dryness. The residue was triturated with acetonitrile (1 mL) and diethyl ether (20 mL) to get a yellowish-orange wax-like solid. The solid was further washed with diethyl ether (20 mL) to obtain the desired product (**3C**) (1.00 g, 1.36 mmol, 63%). ^{1}H NMR ($CDCl_3$, 360 MHz): δ 10.34 (s, 2H); 8.52 (s, 2H); 7.56 (s, 2H); 7.50 (s, 2H); 5.82−5.70 (m, 2H); 5.01−4.92 (m, 4H); 4.42 (t, 4H, J_{H-H} = 7.2 Hz); 4.11 (s, 3H); 2.08−1.94 (m, 8H); 1.45−1.39 (m, 8H). ^{19}F NMR ($CDCl_3$, 339 MHz): δ − 78.51.

Synthesis of ***4C***. Inside the glovebox, an oven-dried Schlenk flask was loaded with $[Ru(p\text{-Cym})Cl_2]_2$ (0.130 g, 0.212 mmol, 1.0 equiv), 1,1′-(4-methoxypyridine-2,6-diyl)bis(3-(hept-6-en-1-yl)-1*H*-imidazol-3-ium)ditriflate (0.296 g, 0.403 mmol, 1.9 equiv), acetonitrile (60 mL) and a stir-bar, the flask was sealed with a rubber septum, taken out of the box and connected to a Schlenk line under N_2. Triethylamine (0.150 mL, 1.06 mmol, 5.0 equiv) was added to the flask using a syringe through the septum. Then the reaction mixture was stirred at 60 °C for 24 h. After cooling to room temperature, the reaction mixture was concentrated to get the crude product into a brownish-yellow solid. The crude product was subjected to column chromatography on silica gel using 0−10% methanol in dichloromethane to get a yellow solid. The solid was triturated three times with a solvent mixture of dichloromethane (1 mL) and diethyl ether (5 mL), the supernatant solution was decanted, and the solid was further washed with diethyl ether (10 mL) to obtain the yellow solid product (**4C**) (0.160 g, 0.200 mmol, 49%). The data supports the presence of triflate as the counteranion based upon ^{19}F NMR and MS in anion mode, but we cannot rigorously rule out the presence of some adventitious chloride anion which would reduce the molecular weight and alter the catalysis TON values slightly. ^{1}H NMR ($CDCl_3$, 360 MHz, ppm): δ 7.86 (d, 2H, J_{HH} = 1.8 Hz); 7.13 (d, 2H, J_{HH} = 1.8 Hz); 7.03 (s, 2H); 5.85−5.74 (m, 2H); 5.03−4.94 (m, 4H); 4.46−4.42 (m, 4H); 4.02 (s, 3H); 2.61 (s, 3H); 2.11−1.98 (m, merged peaks, 11H); 1.52−1.44 (m, 8H). ^{19}F NMR ($CDCl_3$, 339 MHz, ppm): δ −78.18. HRMS (ESI, positive) calculated for $RuC_{30}H_{41}N_7OCl$ [M − $(CF_3SO_3)^-$]$^+$: 652.2105 and found 652.2114. UV−vis: λ_{max} = 359 nm, 401 nm. FTIR (ATR, cm^{-1}): 3084, 2928, 2856, 2271 (CN of nitrile), 1632 (C═C or C═N).

Mass Spectrometry Discussion. To support characterization of the compounds, catalysts **4A**, **4B**, **4C** and **6B** were analyzed by HRMS in positive ion detection mode using ESI. Complex **4A** showed a molecular ion peak at m/z = 622.2017 which is consistent with the calculated value for $RuC_{29}H_{39}N_7Cl$ [M − (CF_3SO_3)]$^+$ = 622.2003. Fragmentation peaks were present at m/z = 540.1479 [M-2CH_3CN]$^+$ (100%) and at m/z = 504.1682 [M-2CH_3CN-HCl]$^+$. Complex **4B** showed a molecular ion peak at m/z = 636.2147 (100%) which is consistent with the calculated value for $RuC_{30}H_{41}N_7Cl$ [M−(CF_3SO_3)]$^+$ = 636.2160. Fragmentation peaks were present at m/z = 554.1641 [M-2CH_3CN]$^+$ (100%) and at m/z = 518.1818 [M-2CH_3CN-HCl]$^+$. Complex **6B** showed a molecular ion peak at m/z = 610.2020 (100%) which is consistent with the calculated value for $RuC_{28}H_{39}N_7Cl$ [M−(CF_3SO_3)]$^+$ = 610.2003. Fragmentation peaks were present at m/z = 569.1723 and 528.1320 corresponding to the loss of one or two CH_3CN molecules. Complex **4C** showed a molecular ion peak at m/z = 652.2114 (100%) which is consistent with the calculated value for $RuC_{30}H_{41}N_7OCl$ [M − (CF_3SO_3)]$^+$ = 652.2105. Fragmentation peaks were present at m/z = 570.1560 [M-2CH_3CN]$^+$ (100%) and at m/z = 534.1770 [M-2CH_3CN-HCl]$^+$.

General Procedure for Photocatalysis. In a 17 mL flame-dried Pyrex glass tube (model #9826) containing a small stir bar, a mixture was prepared consisting of 4 mL of anhydrous acetonitrile (CH_3CN), 0.005 g (0.02 mmol) of BIH, $Ir(ppy)_3$ (1 mL from 0.2 mM CH_3CN stock solution), and Ru catalyst (20 μL from 0.1 mM CH_3CN stock solution) under N_2 atmosphere within an inert glovebox. Each tube was sealed with a screw cap containing a rubber septum and parafilm. The solution was vigorously bubbled with CO_2 for a minimum of 25 min until its volume decreased to 1.9 mL. Following this, 0.1 mL of previously distilled CO_2-degassed triethylamine (NEt_3) was introduced into the mixture to achieve a final volume of 2 mL. The tube was then further sealed using a rubber septum stopper, which was placed over the screw cap and parafilm and secured with copper wire, before the sample was exposed to irradiation from a neutral white light LED lamp (Thorlabs, MNWHL4, color temperature 4900 K) mounted with a collimation adaptor (Thorlabs, SM2F32-A, Lens: Thorlabs, ACL50832U-A, with an antireflective coating range 350−700 nm). The light intensity was set to 180 mW, equivalent to 1 sun, using a Coherent Field Mate power meter equipped with a Coherent PowerMax PM10 detector. To quantify the headspace gas, samples were taken from the sealed glass tube and the pressure was adjusted to atmospheric pressure by compressing a 150 μL headspace sample to 100 μL using a VICI gastight syringe with a stopcock. This syringe was submerged in diethyl ether, and upon opening, gas was observed exiting the needle. After sealing, the syringe was removed from the ether solution and the gas was injected into a PerkinElmer Clarus 680 gas chromatograph equipped with an Agilent Porapak Q column (6 ft. length and 1/8 in. o.d.). Gases were quantified against calibration curves generated using known standards purchased from BuyCalGas.com. CO and CH_4 were quantified using a flame ionization detector equipped with a methanizer, while hydrogen gas was quantified using a thermal conductivity detector. All reported data points are the average of at least 2 experiments with ≤5% deviation from the average.

https://doi.org/10.1021/acs.organomet.4c00282
Organometallics 2024, 43, 2077−2085

■ ASSOCIATED CONTENT

Supporting Information

The Supporting Information is available free of charge at https://pubs.acs.org/doi/10.1021/acs.organomet.4c00282.

Experimental details including spectra, single crystal X-ray diffraction figure (PDF)

Accession Codes

CCDC 2367435 contains the supporting crystallographic data for this paper. These data can be obtained free of charge via www.ccdc.cam.ac.uk/data_request/cif, or by emailing data_request@ccdc.cam.ac.uk, or by contacting The Cambridge Crystallographic Data Centre, 12 Union Road, Cambridge CB2 1EZ, U.K.; fax: +44 1223 336033.

■ AUTHOR INFORMATION

Corresponding Authors

Jonah W. Jurss − *Department of Chemistry, The University of Mississippi, University, Mississippi 38677, United States;* orcid.org/0000-0002-2780-3415; Email: jwjurss@olemiss.edu

Elizabeth T. Papish − *Department of Chemistry, The University of Alabama, Tuscaloosa, Alabama 35487, United States;* orcid.org/0000-0002-7937-8019; Email: etpapish@ua.edu

Authors

Weerachai Silprakob − *Department of Chemistry, The University of Alabama, Tuscaloosa, Alabama 35487, United States*

Jannatul Ferdous − *Department of Chemistry, The University of Mississippi, University, Mississippi 38677, United States*

Sanjit Das − *Department of Chemistry, The University of Alabama, Tuscaloosa, Alabama 35487, United States;* orcid.org/0000-0003-4711-9933

Complete contact information is available at: https://pubs.acs.org/10.1021/acs.organomet.4c00282

Notes

The authors declare no competing financial interest.

■ ACKNOWLEDGMENTS

The authors thank the NSF (CHE-2102416) for funding this research. We thank NSF CHE MRI 1828078 and UA for the purchase of the SC XRD instrument. We thank NSF CHE MRI 1919906 and UA for the purchase of an NMR spectrometer. We thank Dr. Ken Belmore for assistance with the NMR experiments. We thank Jared H. Delcamp and Dinesh Nugegoda for preliminary experiments on this project. J.F. and J.W.J. thank the National Science Foundation for generous funding through a CAREER award (CHE-1848478). We thank Fengrui Qu for single crystal X-ray diffraction analysis on one compound.

■ REFERENCES

(1) Silprakob, W.; Ferdous, J.; Das, S.; Qu, F.; Jurss, J. W.; Papish, E. T. Synthesis, Characterization, and Catalytic CO_2 Reduction Reactivity of Ruthenium CNC Pincer Complexes Containing Macrocyclic or Long Chain Wingtips *ChemRxiv* 2024 DOI: 10.26434/chemrxiv-2024-dgtk3.

(2) Benson, E. E.; Kubiak, C. P.; Sathrum, A. J.; Smieja, J. M. Electrocatalytic and homogeneous approaches to conversion of CO_2 to liquid fuels. *Chem. Soc. Rev.* **2009**, *38* (1), 89−99.

(3) Kunene, T.; Xiong, L.; Rosenthal, J. Solar-powered synthesis of hydrocarbons from carbon dioxide and water. *Proc. Natl. Acad. Sci. U.S.A.* **2019**, *116*, 9693−9695.

(4) Elgrishi, N.; Chambers, M. B.; Wang, X.; Fontecave, M. Molecular polypyridine-based metal complexes as catalysts for the reduction of CO_2. *Chem. Soc. Rev.* **2017**, *46* (3), 761−796.

(5) Luo, Y.-H.; Dong, L.-Z.; Liu, J.; Li, S.-L.; Lan, Y.-Q. From molecular metal complex to metal-organic framework: The CO_2 reduction photocatalysts with clear and tunable structure. *Coord. Chem. Rev.* **2019**, *390*, 86−126.

(6) Morris, A. J.; Meyer, G. J.; Fujita, E. Molecular Approaches to the Photocatalytic Reduction of Carbon Dioxide for Solar Fuels. *Acc. Chem. Res.* **2009**, *42* (12), 1983−1994.

(7) Robert, M. Running the Clock: CO_2 Catalysis in the Age of Anthropocene. *ACS Energy Lett.* **2016**, *1* (1), 281−282.

(8) White, J. L.; Baruch, M. F.; Pander, J. E.; Hu, Y.; Fortmeyer, I. C.; Park, J. E.; Zhang, T.; Liao, K.; Gu, J.; Yan, Y.; Shaw, T. W.; Abelev, E.; Bocarsly, A. B. Light-Driven Heterogeneous Reduction of Carbon Dioxide: Photocatalysts and Photoelectrodes. *Chem. Rev.* **2015**, *115* (23), 12888−12935.

(9) Wang, W.-H.; Himeda, Y.; Muckerman, J. T.; Manbeck, G. F.; Fujita, E. CO_2 Hydrogenation to Formate and Methanol as an Alternative to Photo- and Electrochemical CO_2 Reduction. *Chem. Rev.* **2015**, *115* (23), 12936−12973.

(10) Rodrigues, R. R.; Boudreaux, C. M.; Papish, E. T.; Delcamp, J. H. Photocatalytic Reduction of CO_2 to CO and Formate: Do Reaction Conditions or Ruthenium Catalysts Control Product Selectivity? *ACS Appl. Energy Mater.* **2019**, *2*, 37−46.

(11) Das, S.; Nugegoda, D.; Qu, F.; Boudreaux, C. M.; Burrow, P. E.; Figgins, M. T.; Lamb, R. W.; Webster, C. E.; Delcamp, J. H.; Papish, E. T. Structure Function Relationships in Ruthenium Carbon Dioxide Reduction Catalysts with CNC Pincers Containing Donor Groups. *Eur. J. Inorg. Chem.* **2020**, *2020* (28), 2709−2717.

(12) Das, S.; Nugegoda, D.; Yao, W.; Qu, F.; Figgins, M. T.; Lamb, R. W.; Webster, C. E.; Delcamp, J. H.; Papish, E. T. Sensitized and Self-Sensitized Photocatalytic Carbon Dioxide Reduction Under Visible Light with Ruthenium Catalysts Shows Enhancements with More Conjugated Pincer Ligands. *Eur. J. Inorg. Chem.* **2022**, *2022* (8), No. e202101016.

(13) Yao, W.; Das, S.; DeLucia, N. A.; Qu, F.; Boudreaux, C. M.; Vannucci, A. K.; Papish, E. T. Determining the Catalyst Properties That Lead to High Activity and Selectivity for Catalytic Hydrodeoxygenation with Ruthenium Pincer Complexes. *Organometallics* **2020**, *39* (5), 662−669.

(14) Das, S.; Rodrigues, R. R.; Lamb, R. W.; Qu, F.; Reinheimer, E.; Boudreaux, C. M.; Webster, C. E.; Delcamp, J. H.; Papish, E. T. Highly Active Ruthenium CNC Pincer Photocatalysts for Visible-Light-Driven Carbon Dioxide Reduction. *Inorg. Chem.* **2019**, *58* (12), 8012−8020.

(15) Boudreaux, C. M.; Liyanage, N. P.; Shirley, H.; Siek, S.; Gerlach, D. L.; Qu, F.; Delcamp, J. H.; Papish, E. T. Ruthenium(II) complexes of pyridinol and N-heterocyclic carbene derived pincers as robust catalysts for selective carbon dioxide reduction. *Chem. Commun.* **2017**, *53*, 11217−11220.

(16) Ishida, H.; Fujiki, K.; Ohba, T.; Ohkubo, K.; Tanaka, K.; Terada, T.; Tanaka, T. Ligand effects of ruthenium 2,2′-bipyridine and 1,10-phenanthroline complexes on the electrochemical reduction of CO_2. *J. Chem. Soc., Dalton Trans.* **1990**, 2155−2160.

(17) Tamaki, Y.; Morimoto, T.; Koike, K.; Ishitani, O. Photocatalytic CO_2 reduction with high turnover frequency and selectivity of formic acid formation using Ru(II) multinuclear complexes. *Proc. Natl. Acad. Sci. U.S.A.* **2012**, *109* (39), 15673−15678.

(18) Nakada, A.; Koike, K.; Nakashima, T.; Morimoto, T.; Ishitani, O. Photocatalytic CO_2 Reduction to Formic Acid Using a Ru(II)−Re(I) Supramolecular Complex in an Aqueous Solution. *Inorg. Chem.* **2015**, *54* (4), 1800−1807.

(19) Burks, D. B.; Davis, S.; Lamb, R. W.; Liu, X.; Rodrigues, R. R.; Liyanage, N. P.; Sun, Y.; Webster, C. E.; Delcamp, J. H.; Papish, E. T. Nickel(II) pincer complexes demonstrate that the remote substituent

controls catalytic carbon dioxide reduction. *Chem. Commun.* **2018**, *54*, 3819−3822.
(20) Hawecker, J.; Lehn, J.-M.; Ziessel, R. Photochemical and Electrochemical Reduction of Carbon Dioxide to Carbon Monoxide Mediated by (2,2′-Bipyridine)tricarbonylchlororhenium(I) and Related Complexes as Homogeneous Catalysts. *Helv. Chim. Acta* **1986**, *69* (8), 1990−2012.
(21) Sato, S.; Morikawa, T.; Kajino, T.; Ishitani, O. A Highly Efficient Mononuclear Iridium Complex Photocatalyst for CO_2 Reduction under Visible Light. *Angew. Chem., Int. Ed.* **2013**, *52* (3), 988−992.
(22) Thoi, V. S.; Kornienko, N.; Margarit, C. G.; Yang, P.; Chang, C. J. Visible-Light Photoredox Catalysis: Selective Reduction of Carbon Dioxide to Carbon Monoxide by a Nickel N-Heterocyclic Carbene−Isoquinoline Complex. *J. Am. Chem. Soc.* **2013**, *135*, 14413−14424.
(23) Takeda, H.; Koizumi, H.; Okamoto, K.; Ishitani, O. Photocatalytic CO_2 reduction using a Mn complex as a catalyst. *Chem. Commun.* **2014**, *50* (12), 1491−1493.
(24) Schwartz, T. M.; Burnett, M. E.; Green, K. N. Electronic influence of substitution on the pyridine ring within NNN pincer-type molecules. *Dalton Trans.* **2020**, *49* (7), 2356−2363.
(25) Yao, W.; Olajide, G.; Boudreaux, C. M.; Wysocki, M. M.; Ahmed, M. K.; Qu, F.; Szilvási, T.; Papish, E. T. Cobalt(I) Pincer Complexes as Catalysts for CO_2 Hydrogenation to Formate. *Organometallics* **2024**, *43* (13), 1447−1458.
(26) Andrew, R. E.; Chaplin, A. B. Synthesis and Reactivity of NHC-Based Rhodium Macrocycles. *Inorg. Chem.* **2015**, *54* (1), 312−322.
(27) Andrew, R. E.; Ferdani, D. W.; Ohlin, C. A.; Chaplin, A. B. Coordination Induced Atropisomerism in an NHC-Based Rhodium Macrocycle. *Organometallics* **2015**, *34* (5), 913−917.
(28) Storey, C. M.; Gyton, M. R.; Andrew, R. E.; Chaplin, A. B. Terminal Alkyne Coupling Reactions through a Ring: Mechanistic Insights and Regiochemical Switching. *Angew. Chem., Int. Ed.* **2018**, *57* (37), 12003−12006.
(29) Storey, C. M.; Gyton, M. R.; Andrew, R. E.; Chaplin, A. B. Terminal Alkyne Coupling Reactions Through a Ring: Effect of Ring Size on Rate and Regioselectivity. *Chem. - Eur. J.* **2020**, *26* (64), 14715−14723.
(30) Estrada, A. L.; Jia, T.; Bhuvanesh, N.; Blümel, J.; Gladysz, J. A. Substitution and Catalytic Chemistry of Gyroscope-Like Complexes Derived from Cl−Rh−CO Rotators and Triply trans Spanning Di(trialkylphosphine) Ligands. *Eur. J. Inorg. Chem.* **2015**, *2015* (32), 5318−5321.
(31) Kharel, S.; Joshi, H.; Bhuvanesh, N.; Gladysz, J. A. Syntheses, Structures, and Thermal Properties of Gyroscope-like Complexes Consisting of $PtCl_2$ Rotators Encased in Macrocyclic Dibridgehead Diphosphines $P((CH_2)_n)_3P$ with Extended Methylene Chains (n = 20/22/30) and Isomers Thereof. *Organometallics* **2018**, *37* (18), 2991−3000.
(32) Shima, T.; Hampel, F.; Gladysz, J. A. Molecular Gyroscopes: $\{Fe(CO)_3\}$ and $\{Fe(CO)_2(NO)\}^+$ Rotators Encased in Three-Spoke Stators; Facile Assembly by Alkene Metatheses. *Angew. Chem., Int. Ed.* **2004**, *43* (41), 5537−5540.
(33) Zeits, P. D.; Rachiero, G. P.; Hampel, F.; Reibenspies, J. H.; Gladysz, J. A. Gyroscope-Like Platinum and Palladium Complexes with Trans-Spanning Bis(pyridine) Ligands. *Organometallics* **2012**, *31* (7), 2854−2877.
(34) Cloward, I. N.; Liu, T.; Rose, J.; Jurado, T.; Bonn, A. G.; Chambers, M. B.; Pitman, C. L.; ter Horst, M. A.; Miller, A. J. M. Catalyst self-assembly accelerates bimetallic light-driven electrocatalytic H_2 evolution in water. *Nat. Chem.* **2024**, *16* (5), 709−716.
(35) Shirley, H.; Su, X.; Sanjanwala, H.; Talukdar, K.; Jurss, J. W.; Delcamp, J. H. Durable Solar-Powered Systems with Ni-Catalysts for Conversion of CO_2 or CO to CH_4. *J. Am. Chem. Soc.* **2019**, *141* (16), 6617−6622.
(36) Singh, V.; Singh, R.; Hazari, A. S.; Adhikari, D. Unexplored Facet of Pincer Ligands: Super-Reductant Behavior Applied to Transition-Metal-Free Catalysis. *JACS Au* **2023**, *3* (4), 1213−1220.
(37) Kuyuldar, S.; Burda, C.; Connick, W. B. Tuning two-electron transfer in terpyridine-based platinum(II) pincer complexes. *RSC Adv.* **2019**, *9* (37), 21116−21124.
(38) Roy, S. S.; Talukdar, K.; Jurss, J. W. Electro- and Photochemical Reduction of CO_2 by Molecular Manganese Catalysts: Exploring the Positional Effect of Second-Sphere Hydrogen-Bond Donors. *ChemSusChem* **2021**, *14* (2), 662−670.
(39) Pellegrin, Y.; Odobel, F. Sacrificial electron donor reagents for solar fuel production. *C. R. Chim.* **2017**, *20* (3), 283−295.
(40) Hunt, L. A.; Das, S.; Lamb, R. W.; Nugegoda, D.; Curiac, C.; Figgins, M. T.; Lambert, E. C.; Qu, F.; Hammer, N. I.; Delcamp, J. H.; Webster, C. E.; Papish, E. T. Ruthenium (II) Complexes of CNC Pincers and Bipyridine in the Photocatalytic CO_2 Reduction Reaction to CO Using Visible Light: Catalysis, Kinetics, and Computational Insights. *ACS Catal.* **2023**, *13*, 5986−5999.
(41) Winter, S. M.; Roberts, R. J.; Mailman, A.; Cvrkalj, K.; Assoud, A.; Oakley, R. T. Thermal conversion of a pyridine-bridged bisdithiazolyl radical to a zwitterionic bisdithiazolopyridone. *Chem. Commun.* **2010**, *46* (25), 4496−4498.
(42) Fulmer, G. R.; Miller, A. J. M.; Sherden, N. H.; Gottlieb, H. E.; Nudelman, A.; Stoltz, B. M.; Bercaw, J. E.; Goldberg, K. I. NMR Chemical Shifts of Trace Impurities: Common Laboratory Solvents, Organics, and Gases in Deuterated Solvents Relevant to the Organometallic Chemist. *Organometallics* **2010**, *29* (9), 2176−2179.
(43) Sheldrick, G. M. Crystal structure refinement with SHELXL. *Acta Crystallogr., Sect. C: Struct. Chem.* **2015**, *A71*, 3−8.
(44) Dolomanov, O. V.; Bourhis, L. J.; Gildea, R. J.; Howard, J. A. K.; Puschmann, H. OLEX2: a complete structure solution, refinement and analysis program. *J. Appl. Crystallogr.* **2009**, *42* (2), 339−341.
(45) Sheldrick, G. M. A short history of SHELX. *Acta Crystallogr., Sect. A: Found. Crystallogr.* **2008**, *64*, 112−122.

https://doi.org/10.1021/acs.organomet.4c00282
Organometallics 2024, 43, 2077−2085